SQUID-Based Microwave Cavity Search for Dark-Matter Axions

S. J. Asztalos,* G. Carosi, C. Hagmann, D. Kinion, and K. van Bibber
Lawrence Livermore National Laboratory, Livermore, California 94550, USA

M. Hotz, L. J Rosenberg, and G. Rybka
University of Washington, Seattle, Washington 98195, USA

J. Hoskins, J. Hwang,† P. Sikivie, and D. B. Tanner
University of Florida, Gainesville, Florida 32611, USA

R. Bradley
National Radio Astronomy Observatory, Charlottesville, Virginia 22903, USA

J. Clarke
University of California and Lawrence Berkeley National Laboratory, Berkeley, California 94720, USA
(Received 27 October 2009; published 28 January 2010)

Axions in the μeV mass range are a plausible cold dark-matter candidate and may be detected by their conversion into microwave photons in a resonant cavity immersed in a static magnetic field. We report the first result from such an axion search using a superconducting first-stage amplifier (SQUID) replacing a conventional GaAs field-effect transistor amplifier. This experiment excludes KSVZ dark-matter axions with masses between 3.3 μeV and 3.53 μeV and sets the stage for a definitive axion search utilizing near quantum-limited SQUID amplifiers.

DOI: 10.1103/PhysRevLett.104.041301 PACS numbers: 95.35.+d, 14.80.Va, 95.55.Vj

The axion is a hypothetical particle that may play a central role in particle physics, astrophysics, and cosmology. Axions are pseudoscalars that result from the Peccei-Quinn solution to the strong CP problem [1–3]. Axions or axionlike particles may also be a fundamental feature of string theories [4]. Low-mass axions (m_a in the range of μeV to meV) may have been produced in the early universe in quantities sufficient to account for a large portion of the cold dark matter in galactic halos [5–8]. These dark-matter axions have extremely feeble couplings to normal matter and radiation, but may be converted into detectable microwave photons using the inverse Primakoff effect as first outlined by Sikivie [9,10]. Searches based on this technique are by far the most sensitive for low-mass dark-matter axions. A comprehensive dark-matter axion review can be found in [11]. In this Letter we describe the first results from an axion search that uses a dc SQUID (superconducting quantum interference device), which offers a 2 order of magnitude improvement in the scan rate of our search.

The Axion Dark Matter Experiment (ADMX) has been running in various configurations at Lawrence Livermore National Laboratory (LLNL) since 1996. The ADMX experimental configuration is sketched in Fig. 1. Virtual photons are provided by a 7.6 T magnetic field generated by a large superconducting solenoid with a 0.5 m diameter bore. A cylindrical copper-plated microwave cavity is embedded in the magnet bore, and dark-matter axions passing through the cavity can resonantly convert into real microwave photons with energy $E \approx m_a c^2 + \frac{1}{2} m_a c^2 \beta^2$. With expected velocity dispersions of $\Delta\beta \sim 10^{-3}$ for virialized dark matter in our galaxy, the spread in energy should be $\sim 10^{-6}$ or ~ 1.2 kHz for a 5 μeV axion. The expected power generated by axion-photon conversions is given by [9,10],

$$P_a = g_{a\gamma\gamma}^2 V B_0^2 \rho_a C_{lmn} \min(Q_L, Q_a). \quad (1)$$

Here, $g_{a\gamma\gamma}$ is the coupling strength of the axion to two photons, V is the cavity volume, B_0 is the magnetic field, ρ_a is the local axion dark-matter density, Q_L is the loaded cavity quality factor [(center frequency)/(bandwidth)], $Q_a \sim 10^6$ is the axion signal quality factor [(axion en-

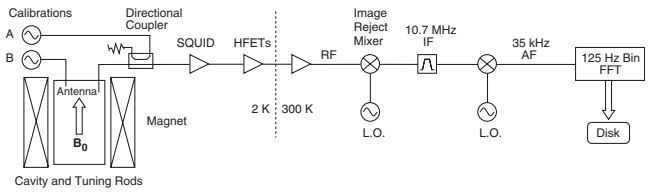

FIG. 1. Schematic of the ADMX experiment. Photons, created in the cavity by the conversion of axions, are picked up by the antenna and amplified by the SQUID and HFETs. The signal is mixed in two stages, with band-limiting filtering between, to audio frequencies. The audio spectrum is measured and stored to disk. Sweep oscillator A provides a reflection measurement to enable adjustment of antenna coupling; oscillator B, weakly coupled, allows measurement of the cavity resonant frequency.

ergy)/(energy spread)] and C_{lmn} is a form factor for the TM_{lmn} cavity mode (overlap of static B field with oscillating E field of the particular mode). In ADMX the TM_{010} mode provides the largest form factor ($C_{010} \approx 0.69$) [12] and its frequency can be scanned between approximately 500 MHz and 1 GHz by translating copper-plated axial tuning rods from the edge of the cavity to the center. The coupling constant $g_{a\gamma\gamma} \equiv g_\gamma \alpha/\pi f_a$, where α is the fine-structure constant, f_a is the "Peccei-Quinn symmetry breaking scale" (an important parameter in axion theory), and g_γ is a dimensionless model-dependent coefficient of O(1). A representative choice within the so-called KSVZ (for Kim-Shifman-Vainshtein-Zakharov) family of models has $g_\gamma \sim 0.97$ [13,14] while one particular choice within the grand unified theory–inspired DFSZ (for Dine-Fischler-Srednicki-Zhitnitskii) family of models has $g_\gamma \sim -0.36$ [15,16]. Given the experimental parameters, a KSVZ axion-photon coupling, and a reasonable local dark-matter density of $\rho_a \approx 0.45\ \mathrm{GeV/cm^3}$ [17], P_a is expected to be of order 10^{-22} W. Detailed experimental descriptions along with previous results can be found in [18,19].

The sensitivity of the detector is set by the Dicke radiometer equation [20] in which the signal-to-noise ratio is

$$\mathrm{SNR} = (P_a/P_N)\sqrt{bt} = (P_a/k_B T_S)\sqrt{t/b}. \quad (2)$$

Here P_N is the system noise power, K_B is Boltzmann's constant, b is the bandwidth, and t is the integration time. The system noise temperature T_S is the sum of the physical cavity temperature T_C and the amplifier noise temperature T_A. In searching the mass range for an axion with a given coupling $g_{a\gamma\gamma}$ at a set SNR the scan rate is given by the amount of bandwidth scanned per unit time. In terms of experimentally adjustable parameters, this scan rate is found from (1) and (2):

$$db/dt \propto dm_a/dt \propto (B_0^2 V)^2/T_S^2 \quad (3)$$

while, given a specific logarithmic scan rate, the smallest detectable coupling ($g_{a\gamma\gamma}^2 \propto P_a$) is given by

$$g_{a\gamma\gamma}^2 \propto (B_0^2 V)^{-1} T_S. \quad (4)$$

Clearly there is a high premium on reducing T_S to its lowest achievable value. Earlier experiments used balanced GaAs heterostructure field-effect transistor (HFET) cryogenic amplifiers built by the National Radio Astronomy Observatory (NRAO) [11,21] for first-stage amplification. HFET amplifiers have noise temperatures that drop as their physical temperature is lowered to around 10 to 20 K, at which point the noise temperature plateaus at a value of a few K. Though extremely quiet by radio astronomy standards, in this application their intrinsic noise of a few K severely limited the scan speed and resolution of the coupling constant in previous experiments. This limitation spurred the development in the late 1990s of replacement amplifiers for ADMX based on dc SQUIDs. Although dc SQUIDs have been used as amplifiers for decades [22], they suffer from severe gain roll-off at microwave frequencies due to parasitic coupling between the input coil and SQUID washer. The SQUID amplifiers developed for ADMX are based on a novel geometry (Fig. 2), where the input coil is replaced by a resonant microstrip input coil [23]. The SQUID amplifier used in the axion search reported here has an *in situ* microwave power gain of ~10 dB in the frequency range scanned.

Unlike HFET amplifiers, the SQUID amplifier noise temperature continues to drop with decreasing temperature until it approaches the quantum noise limit ($T_Q = \hbar\omega/k_B \approx 50$ mK at 1 GHz). Figure 3 shows this behavior for two SQUIDs operating on resonance at 684 and 702 MHz. At the lowest temperatures, their noise temperatures of 47 ± 5 mK are a factor of 1.4 above the quantum-limited noise temperature of 33 mK. Though future experiments will have dilution refrigeration to cool the SQUID and cavity to ~100 mK, the current phase of the experiment used pumped liquid helium (LHe) to maintain cavity and SQUID temperatures of ~2 K. For most of the data run, the cavity was kept under vacuum and cooled via a small LHe reservoir fixed to the cavity top and pumped down to ~1 torr. The SQUID housing was thermally attached via a copper cold finger and copper strap to this reservoir. Regions in frequency where a TE or TEM mode crossed the TM_{010} mode were scanned by filling the cavity with superfluid LHe which shifted the mode crossing by ~3%.

Given its extraordinary flux sensitivity, placing a SQUID amplifier in the strong fringe field of the ADMX magnet provided an additional challenge. To solve this, the SQUID was placed ~1 m above the top of the solenoid where the axial field has diminished to ~0.5 T and inside a superconducting "bucking magnet" solenoid which canceled the fringe field to a few 100 μT. Two nested layers of

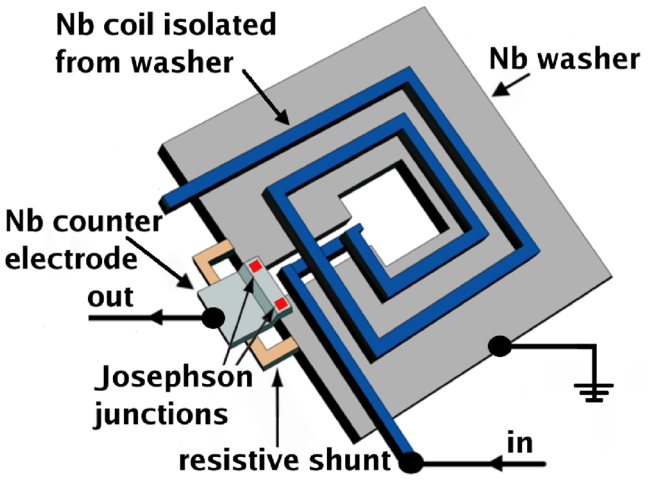

FIG. 2 (color online). Schematic of a microstrip SQUID amplifier.

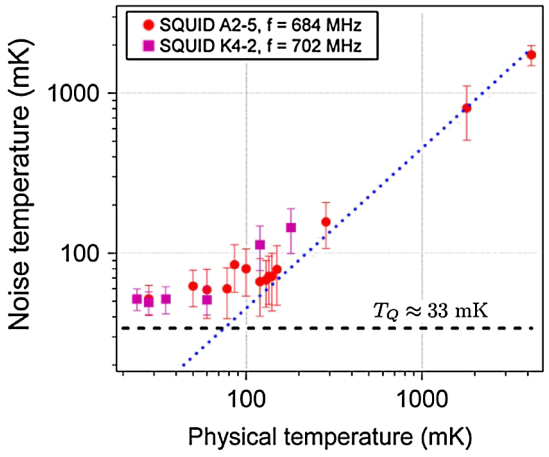

FIG. 3 (color online). Noise temperature of two representative SQUID amplifiers (with resonant frequency f) as a function of physical temperature. Dashed line indicates T_Q, the quantum noise temperature at ≈700 MHz. Dotted line has a unity slope, indicating that $T_A \propto T$ in the classical regime.

cryogenic μ metal further reduced the field during cool down, and the SQUID itself was placed in a superconducting, lead-plated housing to reject any remaining stray field. Hall sensors inside and outside the μ-metal shielding monitored the magnetic fields.

Following the SQUID were second- and third-stage cryogenic HFET amplifiers. These provided an additional 12 dB combined power gain, and contributed a negligible amount to the system noise temperature. The signal was routed via an RG-402 coaxial cable to a room-temperature post-amplifier before being coupled to a double-heterodyne receiver, consisting of an image-rejection mixer with an intermediate frequency (IF) of 10.7 MHz. This IF stage included an eight-pole crystal filter with a 30 kHz bandwidth. The signal was then mixed down a second time with a doubly-balanced mixer to an audio frequency (AF) of 35 kHz. This signal was digitized and analyzed in hardware via fast-Fourier transform (FFT), optimized to search for the fully virialized axion signal. This is our medium resolution channel. At each tuning-rod setting, 10 000 8-msec spectra at 125 Hz Nyquist resolution were added for a total exposure of 80 s. This resulted in a 400 point, single-sided 125 Hz resolution power spectrum. After each 80 s acquisition, the tuning rods moved the TM_{010} mode by ~2 kHz. The loaded Q_L was remeasured before another 80 s acquisition began at the new frequency. The overlap between adjacent spectra was such that each 125 Hz frequency bin had ~25 minutes of exposure.

A high resolution channel, not used in this analysis, is sensitive to axion spectral lines much narrower than 125 Hz. In this channel, after passing through a 6.5-kHz wide passband filter, the 35-kHz signal is mixed to an AF of 5 kHz. This is digitized and a single power spectrum is obtained by acquiring 2^{20} points over 53 s for a Nyquist frequency resolution of 19 mHz. Results from this channel will be described in a future paper.

Each raw power spectrum was corrected for the receiver input-to-output transfer function. The frequency response of the transfer function is dominated by the IF crystal filter, and its effect was determined by an average of many spectra taken over a range of cavity frequency settings. The remaining frequency variation of the transfer function, primarily due to frequency dependent interactions of the cavity, transmission line and amplifier input, was removed by fitting and dividing each spectra by a 6 parameter polynomial. Spectra for which the chi-square of this fit (excluding peaks) was greater than 1.4 were discarded as the receiver transfer function may have been poorly estimated in these cases.

Frequencies were rescanned and the power in the bins averaged until the expected signal-to-noise for a KSVZ axion at a dark-matter density of 0.45 GeV/cm^3 was greater than 3.5. The average signal-to-noise for this run was 10.4, but was allowed to vary between 10 MHz regions. After this, bins of width 125 Hz were examined for excess power above the thermal power level. Additional time was spent rescanning regions with bins that contained too much power to exclude KSVZ axions. True axion signals would be expected to persist and become more statistically significant with more integration time, while statistical fluctuations or transient environmental signals would not. Such rescans were performed within weeks of the original scan, during which a putative axion signal could have shifted at most 20 Hz due to the Earth's orbit and rotation, far smaller than the medium resolution bin width [24]. In this run, the number of rescans agreed with statistical expectations from thermal noise. No signals were found to persist after the second rescan.

The total power and expected axion SNR were used to set a limit on the product of axion coupling and local dark-matter density. Two models for the axion spectral line

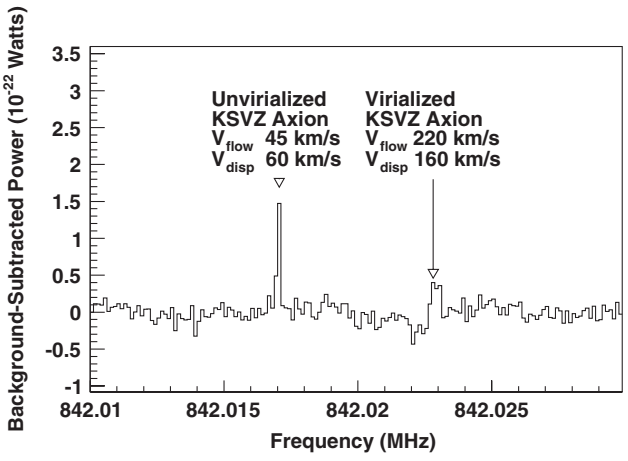

FIG. 4. Dark-matter axion signals simulated with Monte Carlo calculations and imposed on real data for two dark-matter axion distribution models. Example masses chosen to appear at 842.017 MHz and 842.023 MHz.

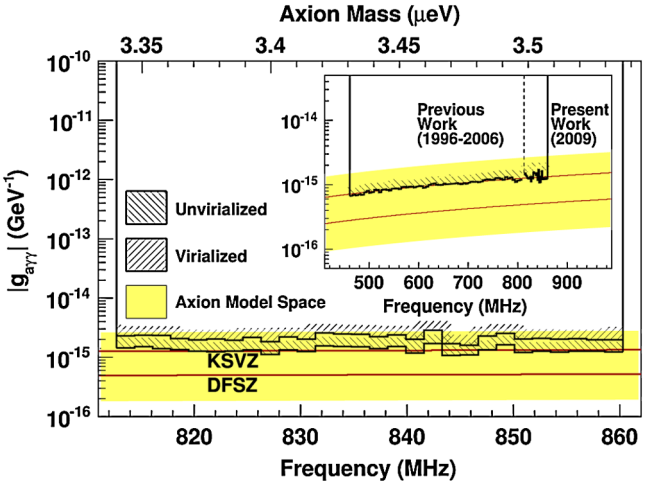

FIG. 5 (color online). Axion-photon coupling excluded at the 90% confidence level assuming a local dark-matter density of 0.45 GeV/cm^3 for two dark-matter distribution models. The shaded region corresponds to the range of the axion-photon coupling models discussed in [28].

shape were examined: completely virialized axions with a velocity dispersion of 160 km/s and a velocity relative to earth of 220 km/s, and axions with a velocity dispersion and relative velocity of 60 km/s or less, as would be predicted by a caustic model [25] or a dark disk model [26]. Expected signals for both models superimposed on real data are shown in Fig. 4. Models with lower velocity dispersions produce narrower peaks in the power spectrum, with a consequently higher SNR. The 90% confidence bound on axion coupling with a local dark-matter density of 0.45 GeV/cm^3 is shown in Fig. 5, set with the Monte Carlo method outlined in [27].

We exclude at 90% confidence realistic axion models of dark matter, with a local density of 0.45 GeV/cm^3 for axion masses ranging 3.3 μeV to 3.53 μeV. This extends the excluded region from that covered in Ref. [19], excluding plausible axion dark-matter models from 1.9 μeV to 3.53 μeV. Furthermore, we have demonstrated the first application of a dc SQUID amplifier in the high field environment of the axion detector with a noise temperature comparable to our previous runs with the HFET amplifier. While the scan rate over this range was not significantly enhanced, in the next phase of ADMX, the SQUID and cavity will be cooled with a dilution refrigerator to 100 mK. At this temperature, the scan rate should be improved so that the entire first decade of mass for the more weakly-coupled DSFZ axions, a factor of 7 greater sensitivity, can be explored in roughly two years of continuous running.

This research is supported by the U.S. Department of Energy, Office of High Energy Physics under Contracts No. DE-FG02-96ER40956 (Lawrence Livermore National Laboratory), No. DE-AC52-07NA27344 (University of Washington), and No. DE-FG02-97ER41029 (University of Florida). Additional support was provided by Lawrence Livermore National Laboratory under the LDRD program. The National Radio Astronomy Observatory is a facility of the National Science Foundation operated under cooperative agreement by Associated Universities, Inc. Development of the SQUID amplifier (J. C.) was supported by the Director, Office of Science, Office of Basic Energy Sciences, Materials Sciences and Engineering Division, of the U.S. Department of Energy under Contract No. DE-AC02-05CH11231.

*Present address: XIA LLC, 31057 Genstar Road, Hayward CA, 94544, USA.
†Present address: Pusan National University, Busan, 609-735, Republic of Korea.

[1] R. D. Peccei and H. R. Quinn, Phys. Rev. Lett. **38**, 1440 (1977).
[2] S. Weinberg, Phys. Rev. Lett. **40**, 223 (1978).
[3] F. Wilczek, Phys. Rev. Lett. **40**, 279 (1978).
[4] P. Svřcek and E. Witten, J. High Energy Phys. 06 (2006) 051.
[5] J. Preskill, M. Wise, and F. Wilczek, Phys. Lett. B **120**, 127 (1983).
[6] L. F. Abbott and P. Sikivie, Phys. Lett. B **120**, 133 (1983).
[7] M. Dine and W. Fischler, Phys. Lett. B **120**, 137 (1983).
[8] J. Ipser and P. Sikivie, Phys. Rev. Lett. **50**, 925 (1983).
[9] P. Sikivie, Phys. Rev. Lett. **51**, 1415 (1983).
[10] P. Sikivie, Phys. Rev. D **32**, 2988 (1985).
[11] R. Bradley *et al.*, Rev. Mod. Phys. **75**, 777 (2003).
[12] H. Peng *et al.*, Nucl. Instrum. Methods Phys. Res., Sect. A **444**, 569 (2000).
[13] J. Kim, Phys. Rev. Lett. **43**, 103 (1979).
[14] M. Shifman, A. Vainshtein, and V. Zakharov, Nucl. Phys. B **166**, 493 (1980).
[15] A. Zhitnitskii, Sov. J. Nucl. Phys. **31**, 260 (1980).
[16] M. Dine, W. Fischler, and M. Srednicki, Phys. Lett. B **104**, 199 (1981).
[17] E. Gates, G. Gyuk, and M. Turner, Astrophys. J. **449**, L123 (1995).
[18] L. D. Duffy *et al.*, Phys. Rev. D **74**, 012006 (2006).
[19] S. J. Asztalos *et al.*, Phys. Rev. D **69**, 011101 (2004).
[20] R. Dicke, Rev. Sci. Instrum. **17**, 268 (1946).
[21] E. Daw and R. Bradley, J. Appl. Phys. **82**, 1925 (1997).
[22] J. Clarke, A. Lee, M. Mück, and P. Richards, in *The SQUID Handbook Vol. II: Applications of SQUIDs and SQUID Systems* (Wiley-VCH, Weinheim, Germany, 2006), pp. 1–93.
[23] M. Mück, M.-O. Andŕe, J. Clarke, J. Gail, and C. Heiden, Appl. Phys. Lett. **72**, 2885 (1998).
[24] F.-S. Ling, P. Sikivie, and S. Wick, Phys. Rev. D **70**, 123503 (2004).
[25] L. D. Duffy and P. Sikivie, Phys. Rev. D **78**, 063508 (2008).
[26] J. I. Read, G. Lake, O. Agertz, and V. P. Debattista, Mon. Not. R. Astron. Soc. **389**, 1041 (2008).
[27] S. Asztalos *et al.*, Phys. Rev. D **64**, 092003 (2001).
[28] J. E. Kim, Phys. Rev. D **58**, 055006 (1998).